THE JOURNAL OF BIOLOGICAL CHEMISTRY VOL. 281, NO. 15, pp. 10516–10526, April 14, 2006

Vitamin D Receptor Agonists Specifically Modulate the Volume of the Ligand-binding Pocket*[S]

Received for publication, December 21, 2005, and in revised form, February 6, 2006 Published, JBC Papers in Press, February 13, 2006, DOI 10.1074/jbc.M513609200

Ferdinand Molnár[‡], Mikael Peräkylä[§], and Carsten Carlberg[‡1]

From the [‡]Department of Biochemistry and the [§]Department of Chemistry, University of Kuopio, FIN-70211 Kuopio, Finland

Existing crystal structure data has indicated that 1α,25-dihydroxyvitamin D_3 (1α,25$(OH)_2D_3$) and its analogues bind the ligand-binding pocket (LBP) of the human vitamin D receptor in a very similar fashion. Because docking of a ligand into the LBP is a more flexible process than crystallography can monitor, we analyzed 1α,25$(OH)_2D_3$, its 20-epi derivative MC1288, the two side-chain analogues Gemini and Ro43-83582 (a hexafluoro-derivative) by molecular dynamics simulations in a complex with the vitamin D receptor ligand-binding domain and a co-activator peptide. Superimposition of the structures showed that the side chain of MC1288, the first side chain of the conformation II of Gemini, the second side chain of Ro43-83582 in conformation I and the first side chain of Ro43-83582 in conformation II take the same agonistic position as the side chain of 1α,25$(OH)_2D_3$. Compared with the LBP of the natural hormone MC1288 reduced the volume by 17%, and Gemini expanded it by 19%. The shrinking of the LBP of MC1288 and its expansion to accommodate the second side chain of Gemini or Ro43-83582 is the combined result of minor movements of more than 30 residues and major movements of a few critical amino acids. The agonist-selective recognition of anchoring OH groups by the conformational flexible residues Ala-303, Leu-309, and His-397 was confirmed by *in vitro* assays. In summary, variations in the volume of agonists lead to adaptations in the volume of the LBP and alternative contacts of anchoring OH-groups.

The nuclear receptor for the seco-steroid 1α,25$(OH)_2D_3$, VDR,[2] is one of the classic 11 endocrine members of the nuclear receptor superfamily, which binds its ligand with high affinity (K_d value of 0.1 nM) (1). Like most nuclear receptors, VDR has a highly conserved DNA-binding domain and a structurally conserved ligand-binding domain (LBD). The 12 α-helices of the LBD form a three-layered anti-parallel sandwich, which comprises a central core layer of the helices 5, 9, and 11 that is sandwiched between two additional layers of helices creating a LBP (2). The interior surface of the LBP is mostly made up of non-polar amino acids and thereby complements the hydrophobic character of VDR ligands. Specificity is achieved through a limited number of hydrogen bonds between the 1-OH group and Ser-237 (helix 3)/Arg-274 (helix 5), the 3-OH-group and Ser-278 (helix 5)/Tyr-143 (helix 1), and the 25-OH-group and His-305 (loop between helices 6 and 7)/His-397 (helix 11) (3).

VDR acts preferentially as a heterodimer with the retinoid X receptor (RXR) on specific DNA sequences in promoter regions of 1α,25$(OH)_2D_3$ target genes, referred to as 1α,25$(OH)_2D_3$ response elements (VDREs) (4). VDR·RXR·VDRE complexes are the molecular cores of DNA-dependent 1α,25$(OH)_2D_3$ signaling (5), and the stabilization of the agonistic VDR LBD conformation is the most critical step in this signaling process. Comparison of the structure of the apo-RXR (6) with the ligand-bound retinoid acid receptor (7) suggested that receptors undergo a specific switch between two conformations, which involves a major rearrangement of helix 12 as well as a number of more subtle changes. In the agonistic conformation the LBD interacts with co-activator (CoA) proteins, such as SRC-1, TIF2, and RAC3 (8). CoA proteins contain multiple, short receptor interaction domains, with the central sequence L*XX*LL (9). The receptor interaction domain of the CoA makes contacts with helices 3, 4, and 12 of the LBD, which are stabilized by a charge clamp between Glu-420 (helix 12) and Lys-246 (helix 3) (10, 11).

1α,25$(OH)_2D_3$ is a key player in calcium homeostasis and bone mineralization (12) but also has anti-proliferative and pro-differentional effects on various cell types (13). More than 3000 synthetic analogues of 1α,25$(OH)_2D_3$ are presently known, and the majority of them carry a modification in their aliphatic side chain (14). 1α,25$(OH)_2D_3$ analogues have been developed with the goal of improving the biological profile of the natural hormone for therapeutic application either in hyperproliferative diseases, such as psoriasis and different types of cancer, or in bone disorders, such as osteoporosis (15). Most of the analogues described to date are agonists, with a few having been identified as antagonists. An interesting exception is Gemini, which is the first 1α,25$(OH)_2D_3$ analogue that carries two side chains (16, 17) and subsequently has an ~20% higher volume than the natural hormone.

The most detailed information about the molecular mechanisms of the analogues can be obtained from crystal structures. The human VDR LBD has been crystallized with the natural hormone, its 20-epi analogue MC1288, and a few other synthetic agonists (18–21), but neither with antagonists nor with Gemini (although there is preliminary information on the zebrafish VDR-LBD-Gemini structure (22)). Molecular dynamics (MD) simulations of the Gemini-VDR showed that the analogue can bind the VDR LBD in two different conformations (23). In one of these conformations Gemini acts as an agonist with one side chain taking the same position as that of the natural hormone. In contrast, in its other conformation Gemini acts as an inverse agonist, because both of its side chains take alternative positions to that of 1α,25$(OH)_2D_3$ (24). In analogy to a number of one side-chain analogues, the addition of fluorine atoms improved the potential of Gemini even more (23, 25). Taken together, the LBP of the VDR seems to be flexible enough to accommodate large ligands, such as Gemini and its derivatives.

* This work was supported by The Academy of Finland, the Finnish Cancer Organization, and the Kuopio University Pharmacy Fund (to C. C.). The costs of publication of this article were defrayed in part by the payment of page charges. This article must therefore be hereby marked "*advertisement*" in accordance with 18 U.S.C. Section 1734 solely to indicate this fact.

[S] The on-line version of this article (available at http://www.jbc.org) contains supplemental Tables S1 and S2 and Fig. S3.

[1] To whom correspondence should be addressed: Dept. of Biochemistry, University of Kuopio, P.O. box 1627, FIN-70211 Kuopio, Finland. Tel.: 358-17-163062; Fax: 358-17-2811510; E-mail: carlberg@messi.uku.fi.

[2] The abbreviations used are: VDR, 1α,25$(OH)_2D_3$ receptor; CoA, co-activator; GST, glutathione *S*-transferase; MD, molecular dynamics; RXR, retinoid X receptor; LBD, ligand-binding domain; LBP, ligand-binding pocket; SOM, self-organizing map; TIF2, transcription intermediary factor 2; VDRE, 1α,25$(OH)_2D_3$ response element; wt, wild type; Gemini, 21-(3-OH-methyl-butyl)-1α,25$(OH)_2D_3$; Ro43-83582, 21-(3-OH-methyl-butyl)-23-yne-26,27-F_6-1α,25$(OH)_2D_3$.

The docking of a ligand into the LBP is probably a much more dynamic process than "static" crystallography can monitor. In this study we therefore analyzed 1α,25(OH)$_2$D$_3$, MC1288, Gemini, and Ro43-83582 by MD simulations in a complex with VDR and a CoA peptide. Superimposition of the structures revealed details about the position of the side chains of the ligand and the amino acids forming the LBP. These investigations led to the observation that MC1288 reduced the volume of the LBP by 17%, whereas Gemini expanded it by 19%. We also found agonist-selective recognition of anchoring groups by the conformational flexible residues Ala-303, Leu-309, and His-397 and confirmed them by *in vitro* assays.

EXPERIMENTAL PROCEDURES

VDR Ligands—1α,25(OH)$_2$D$_3$ and MC1288 (20-epi-1α,25(OH)$_2$D$_3$) were a gift from Dr. L. Binderup (Leo Pharma, Ballerup, Denmark), and Gemini (21-(3-OH-methyl-butyl)-1α,25(OH)$_2$D$_3$) and Ro43-83582 (21-(3-OH-methyl-butyl)-23-yne-26,27-F$_6$-1α,25(OH)$_2$D$_3$), a Gemini derivative (23, 25), were kindly provided by Dr. Milan Uskokovic (BioXell, Inc., Nutley, NJ). The VDR ligands were dissolved in 2-propanol and further dilutions were made in Me$_2$SO (for *in vitro* experiments) or in ethanol (for cell culture experiments).

Protein Expression Vectors—Full-length cDNAs for human VDR (26) and human RXRα (27) were subcloned into the T7/SV40 promoter-driven pSG5 expression vector (Stratagene, Heidelberg, Germany). The point mutants of human VDR were generated using the QuikChange™ site-directed mutagenesis kit (Stratagene) according to the manufacturer's instructions. All mutations were confirmed by sequencing. The same constructs were used for both T7 RNA polymerase-driven *in vitro* transcription/translation of the respective cDNAs and for viral promoter-driven overexpression of the respective proteins in mammalian cells.

GST Fusion Protein Constructs—The receptor interaction domain of human TIF2 (spanning residues 646–926) (28) was subcloned into the GST fusion vector pGEX (Amersham Biosciences).

Reporter Gene Constructs—Four copies of DR3-type VDRE of the rat atrial natriuretic factor gene (core sequence AG**AGGTCA**TGA**AGGACA**) (29) were fused with the thymidine kinase minimal promoter driving the firefly luciferase reporter gene.

Structural Modeling and MD Simulations—The initial coordinates of VDR were obtained from the crystal structure of the VDR·LBD·1α,25(OH)$_2$D$_3$ complex (Protein Data Bank code 1DB1) (18). The amino acids missing from the x-ray structure (residues 118, 119, 375–377, and 424–427) were built using the Quanta98 molecular modeling package (Molecular Simulations Inc., San Diego, CA). The four residues missing from the C terminus (residues 424–427) were built in an α-helical conformation ($\phi = -57°$, $\psi = -47°$). The CoA peptide KNHPMLMNLLKDN was added to the simulation system and placed on the surface of the VDR LBD on the basis of rat VDR·LBD·1α,25(OH)$_2$D$_3$ complex crystal structure (1RK3) (11). 1α,25(OH)$_2$D$_3$ was placed to the LBP using the VDR·LBD·1α,25(OH)$_2$D$_3$ crystal structure as a model. Gemini and Ro43-83582 were docked in two different conformations to VDR on the basis of earlier MD simulation results (23). For the energy minimizations and MD simulations the VDR complexes were hydrated with TIP3P water molecules in a periodic box of ~61 × 69 × 86 Å. Crystallographic water molecules were included in the simulation systems. The water molecules of the complexes were first energy-minimized for 1000 steps, heated to 300 K in 5 ps, and equilibrated by 10 ps at constant volume and temperature of 300 K. After that the simulation systems were minimized for 1000 steps, the temperature of the systems was increased to 300 K in 5 ps, and equilibrated for 100 ps. The equilibration was carried out at constant pressure (1 atm) conditions. After that production simulations of 1 ns were started. In the simulations the electrostatics were treated using the particle-mesh Ewald method. A time step of 1.5 fs was used, and bonds involving hydrogen atoms were constrained to their equilibrium lengths using the SHAKE algorithm. The simulations were done using the AMBER8.0 simulation package (University of California, San Francisco, CA) and the parm99 parameter set of AMBER. The parameters of the ligands were generated with the Antechamber suite of AMBER8.0 in conjunction with the general amber force field. The atomic point charges of the ligands were calculated with the two-stage RESP fit (30) at the HF/6-31G* level using ligand geometries optimized with the semi-empirical PM3 method using the Gaussian03 program (Gaussian Inc., Pittsburgh, PA).

Self-organizing Maps (SOMs)—Visual Data software (Visipoint Oy, Kuopio, Finland) is based on SOMs, which are artificial neural network algorithms in the unsupervised learning category that can visualize and interpret large high dimensional data sets (31). The map consists of a regular grid of processing units, so-called "neurons." A model of some multidimensional observation, eventually a vector consisting of features, is associated with each unit. The map attempts to represent all of the available observations with optimal accuracy using a restricted set of models. At the same time the models become ordered on the grid so that similar models are close to each other and dissimilar models far from each other. The input data for SOM are the distances of amino acid residues in the complexes of VDR with MC1288, Gemini (in conformations I and II), and Ro43-83582 (in conformations I and II) compared with that with 1α,25(OH)$_2$D$_3$. All values were used as the training pattern. At the beginning, each neuron of the SOM was randomly assigned a weight vector with five variables using 1024 as a starting maximal resolution. The weight vectors of the best matching neuron and its neighbors are moved toward the values of the input vectors such that neurons come to represent a group of amino acids with similar conformational flexibility. During the training the adjustment of weight vectors diminished. Then each amino acid is placed into a neuron, which best describes its flexibility pattern profile, and the value of difference is displayed on each neuron as a bar graph. The resulted map with matrix resolution 16 × 16 was changed to 4 × 4 to exclude empty clusters in the matrix. Finally, a Sammon's mapping algorithm (Visipoint Oy) was applied to visualize the clustered groups in n-dimensional space in two dimensions.

LBP and Ligand Volume Calculations—The volume of the LBP was calculated with Voidoo software (Uppsala Software Factory, Uppsala, Sweden). The probe radius in the calculations was set to 1.9 Å. For mesh representation the grid for plot files was set as 0.5 Å and for iso-surfaces as 0.2 Å. The obtained graphical representation EZD file output was converted with MAPMAN software (Uppsala Software Factory) to DSN6 FRODO format electron density maps. The maps were loaded, visualized, and rendered in MacPyMOL (DeLano Scientific LLC). Ligand volumes were calculated by the molecular modeling software SYBYL (Tripos Inc., St. Louis, MO) from the Connolly surfaces of the ligands that were created using a probe radius of 1.4 Å.

In Vitro Translation and Bacterial Overexpression of Proteins—In vitro translated wild type or mutated human VDR and RXR proteins were generated by coupled *in vitro* transcription/translation using rabbit reticulocyte lysate as recommended by the supplier (Promega, Madison, WI). Protein batches were quantified by test translations in the presence of [^{35}S]methionine. The specific concentration of the receptor proteins was adjusted to ~4 ng/μl after taking the individual number of methionine residues/protein into account. Bacterial overexpression of GST-TIF2$_{646-926}$ was obtained from the *Escherichia coli* BL21(DE3)pLysS strain (Stratagene) containing the respective expression plasmids. Overexpression was stimulated with 0.25 mM isopropyl-β-D-thio-galactopyranoside

for 3 h at 37 °C, and the proteins were purified and immobilized on glutathione-Sepharose 4B beads (Amersham Biosciences) according to the manufacturer's protocol. Proteins were eluted in the presence of glutathione.

Transient Transfections and Luciferase Reporter Gene Assays—MCF-7 human breast cancer cells were seeded into 6-well plates (200,000 cells/well) and grown overnight in phenol red-free Dulbecco's modified Eagle's medium supplemented with 5% charcoal-stripped fetal bovine serum. Plasmid DNA containing liposomes were formed by incubating 100 ng of an expression vector for wild type or mutant VDR and 1 μg of reporter plasmid with 10 μg of *N*-[1-(2,3-dioleoyloxy)propyl]-*N*,*N*,*N*-trimethylammonium methylsulfate (DOTAP, Roth, Karlsruhe, Germany) for 15 min at room temperature in a total volume of 100 μl. After dilution with 900 μl of phenol red-free Dulbecco's modified Eagle's medium, the liposomes were added to the cells. Phenol red-free Dulbecco's modified Eagle's medium supplemented with 500 μl of 15% charcoal-stripped fetal bovine serum was added 4 h after transfection. Also at this time, VDR agonists (final concentration 1 nM) or solvent was added. The cells were lysed 16 h after the onset of stimulation using reporter gene lysis buffer (Roche Diagnostics), and the constant light signal luciferase reporter gene assay was performed as recommended by the supplier (Canberra-Packard, Groningen, The Netherlands). The luciferase activities were normalized with respect to protein concentration.

Limited Protease Digestion Assay—In vitro translated, ^{35}S-labeled wild type or mutated human VDR (20 ng) was incubated with Me_2SO or VDR agonists (final concentration 1 μM) for 15 min at room temperature in a total volume of 10 μl. Trypsin (Promega, final concentration 100 ng/μl) was then added, and the incubation was continued for 30 min at room temperature. The limited proteolysis was stopped by adding one volume of protein gel loading buffer (0.25 M Tris, pH 6.8, 20% glycerol, 5% mercaptoethanol, 2% SDS, 0.025% bromphenol blue). The samples were denatured for 3 min at 95 °C, resolved by electrophoresis through 15% SDS-polyacrylamide gels, and visualized on a FLA3000 reader (Fuji, Tokyo, Japan) using ScienceLab99 software (Fuji).

Supershift Assays—Supershift assays were performed with equal amounts (10 ng) of *in vitro* translated wild type or mutant human VDR and RXRα. The proteins were incubated for 15 min with Me_2SO or VDR agonists (final concentration 1 μM) in a total volume of 20 μl of binding buffer (10 mM Hepes, pH 7.9, 150 mM KCl, 1 mM dithiothreitol, 0.2 μg/μl poly(dI-dC), and 5% glycerol). Bacterially expressed GST-TIF2$_{646-926}$ fusion protein was added to the reaction mixture. Approximately 1 ng of ^{32}P-labeled double-stranded oligonucleotides (50,000 cpm) corresponding to one copy of the DR4-type VDRE of the rat *pit-1* gene (core sequence GA**AGTTCA**TGAG**AGTTCA**) (32) was then added, and the incubation was continued for 15 min at room temperature. Protein·DNA complexes were resolved by electrophoresis through 8% non-denaturing polyacrylamide gels in 0.5 × TBE (45 mM Tris, 45 mM boric acid, 1 mM EDTA, pH 8.3) and visualized on a FLA3000 reader using ScienceLab99 software.

RESULTS

Side Chain Orientations of VDR Agonists—The VDR ligand 1α,25(OH)$_2$D$_3$, its 20-epi derivative MC1288 (33, 34) and Gemini (16, 17) carry unmodified side chains (Fig. 1*A*). In contrast, Ro43-83582 contains six electronegative fluorine atoms at C-31 and C-32 and carries a triple bond between C-28 and C-29 (Fig. 1*A*). We performed MD simulations for each of the four ligands in a complex with the VDR LBD and a CoA peptide. The simulations were started on coordinates of the crystal structure of the human VDR LBD (18), which has been completed by molecular modeling with the residues 118, 119, 375–377, and 424–427. The coordinates of the CoA peptide were obtained from a complex with the rat VDR LBD (1RK3 (11)). As expected, for both Gemini and Ro43-83582 two conformations, I and II, were obtained. The MD simulation structures of the complexes with MC1288, Gemini, and Ro43-83582 (both in two conformations) were individually superimposed with the simulated VDR·1α,25(OH)$_2$D$_3$ complex. From these superimpositions only the ligand structures are shown (Fig. 1*B*). A superimposition of the VDR·1α,25(OH)$_2$D$_3$ (1DB1 (18)) and the VDR·MC1288 (1IE9 (19)) crystal structures served as a reference for the quality of the MD simulations. However, it should be noted that the latter crystal structure complexes did not contain any CoA peptide.

In general, all four agonists took similar positions within the LBP of the receptors, although Gemini and Ro43-83582 had to find space for their additional side chains. For a more detailed analysis the distances between the C-25 atoms of the (first) side chains of all four ligands and, in case of Gemini and Ro43-83582, also that to the C-30 atoms of the second side chain were determined (Fig. 1*B*). The distances between the C-25 atoms of 1α,25(OH)$_2$D$_3$ and MC1288 were found to be 0.4 Å based on the crystal structures and 1.0 Å according to our MD simulations. When Gemini was in conformation I (Fig. 1*B*, *orange*) the C-25 atom resident in the first side chain had a distance of 3.7 Å compared with that of 1α,25(OH)$_2$D$_3$, whereas the C-30 atom of the second side chain of Gemini showed only a distance of 2.1 Å compared with the C-25 atom of the natural ligand. In conformation II (Fig. 1*B*, *blue*) the first side chain of Gemini took nearly the same position as the side chain of 1α,25(OH)$_2$D$_3$ with a deviation of only 0.7 Å in their C-25 atoms. In contrast, in the conformation II of Gemini the C-30 atom of the second side chain showed the large distance of 6.9 Å to the C-25 atom of the natural ligand. Interestingly, in conformation I of Ro43-83582 (*orange*) the C-25 atom of the first side chain was in a distance of even 7.4 Å to the respective carbon atom of 1α,25(OH)$_2$D$_3$, whereas the C-30 atom of the second side chain deviated only by 0.9 Å. The C-25 atom of first side chain of conformation II of Ro43-83582 (*blue*) had only a distance of 0.6 Å to that of the natural ligand, whereas the C-30 atom of the second side chain was in a distance of 7.3 Å. For each of the four VDR agonists the distances between their anchoring OH-groups are indicated in supplemental Table S1. Taken together, the side chain of MC1288, the first side chain of the conformation II of Gemini, the second side chain of Ro43-83582 in conformation I, and the first side chain of Ro43-83582 in conformation II take nearly the same position as the side chain of the natural ligand.

An Analysis of the Amino Acids Lining the VDR LBP—We determined the impact of individual amino acids on the shape of the LBP of the VDR with the program Voidoo. In the five superimpositions of the MD simulation structures of VDR with MC1288, Gemini (in conformations I and II), and Ro43-83582 (in conformations I and II) with that of the VDR·1α,25(OH)$_2$D$_3$ complex, we measured for each of the 40 amino acid residues forming the LBP the average distance between the respective most terminal atoms (excluding hydrogens). In the case of aromatic residues we considered the average distance of all ring atoms and in the case of branched residues, the average of both terminal atoms. These 200 values (between 0.08 and 6.13 Å, see supplemental Table S2) form a five-dimensional data set. SOM clustering allowed the sorting of the 40 residues of the LBP into 16 groups (Fig. 2). In each group are those amino acids that showed comparable ligand-induced movements. Amino acids with more profound conformational flexibility were found in the peripheral groups I–X, whereas groups XI–XVI form the center of the map and contain residues that show only minor differences in their positions in the different VDR-agonists structures. The location of

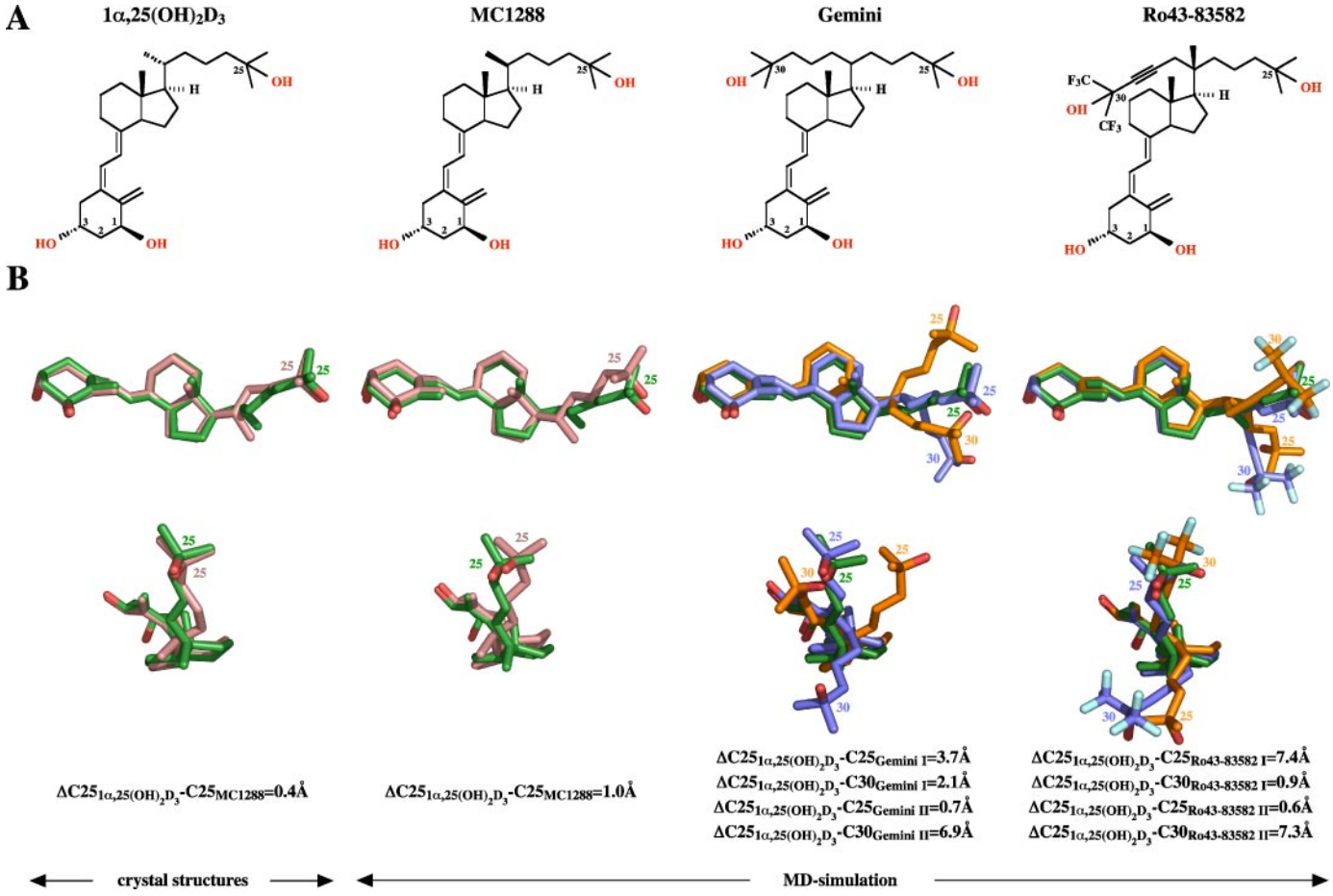

FIGURE 1. **Orientation of side chains of VDR agonists.** The chemical formulas of the VDR agonists used for MD simulations are shown (*A*). The superimposed three-dimensional agonist structures are derived from crystal structures (*far left*) or from MD simulations (*B*). Please note that the MD simulations were performed in the presence of CoA peptide, whereas the crystal structures were solved without. $1\alpha,25(OH)_2D_3$ is color-coded in *green*, MC1288 in *light brown*, and Gemini and Ro43-83582 in conformation I in *orange* and in conformation II in *blue*. *Top* and *bottom* each represents the same molecule turned by 90°. The distances between the C-25 atoms of $1\alpha,25(OH)_2D_3$ compared with that of the C-25 and C-30 atoms of the superimposed ligands are indicated below the respective structures. *Dashed lines* link corresponding side chains of the two conformations of Gemini and Ro43-83582.

all 40 amino acids is shown in supplemental Fig. S3. Taken together, SOM clustering allows us to sort the amino acids forming the LBP into a group of a few more flexible representatives close to the side chain of the agonists and the less flexible majority of residues that fix, rather unspecifically, the ring system of the ligands.

Ligand-dependent Modulation of the LBP Volume—The volumes of the four ligands (Gemini and Ro43-83582 in both of their conformations) and of their corresponding LBPs were calculated using SYBYL and Voidoo software packages, respectively (Table 1). The ligand volumes range from 427.3 $Å^3$ (representing 98.5% of the volume of $1\alpha,25(OH)_2D_3$) for MC1288 to 541.7 $Å^3$ (124.8%) for Ro43-83582 in conformation II. Interestingly, the volume of the VDR LBP did not remain constant and varied between 643.0 $Å^3$ for the complex with MC1288 and 919.6 $Å^3$ for that with Gemini in conformation II. In general, a larger ligand results in an increased size of the LBP, but this relation is not very strict. The natural ligand, as well as Gemini in conformation II, occupied ~56% of their LBP space, whereas MC1288 and Ro43-83582 in conformation I filled ~67% of the LBP. For Gemini in conformation I and Ro43-83582 in conformation II an intermediate occupancy rate was found (62.8 and 63.7%, respectively).

In summary, the volume of the LBP of the VDR was found to be flexible and appears to adapt to variations in the volume of the ligand. However, these adoptions are not strictly proportional and result for some ligands, such as Ro43-83582 in conformation I and MC1288, in a more efficient occupancy of the LBP.

Visualization of the LBP Flexibility—To visualize the above described ligand-dependent adaptations of the LBP volume, the iso-surface rendered LBPs of the complexes of VDR with MC1288, Gemini (conformations I and II), and Ro43-83582 (conformations I and II) were superimposed with the LBP of the VDR·$1\alpha,25(OH)_2D_3$ complex (Fig. 3, *green*). In addition, the representative amino acids His-397, Phe-422, Leu-309, Tyr-295, Ala-303, and Phe-150 are shown in the same color code. For MC1288 the differences are rather minor, and representative amino acids shift their position in maximum by 1.2 Å. However, these movements are all toward the ligand and indicate a shrinking of the LBP of MC1288. Similarly, the excess of green color on the surface of the superimposition indicates that the LBP of $1\alpha,25(OH)_2D_3$ is larger than that of its 20-epi derivative.

In conformation I of Gemini, the residues His-397, Phe-422, and Tyr-295 made shifts of 6.13, 3.44, and 3.14 Å, respectively, which increased the volume of the LBP around the aliphatic side chains of the ligand. In contrast, Phe-150, which is close to the A-ring, showed only a minor movement of 1.08 Å. In contrast, the LBP of Gemini in conformation II resembled more closely that of $1\alpha,25(OH)_2D_3$, and Tyr-295 made the largest movement with 3.00 Å. However, the most critical event seems to be the shift of Leu-309 by 2.74 Å, which allowed the accommodation of the second side chain in an extended LBP.

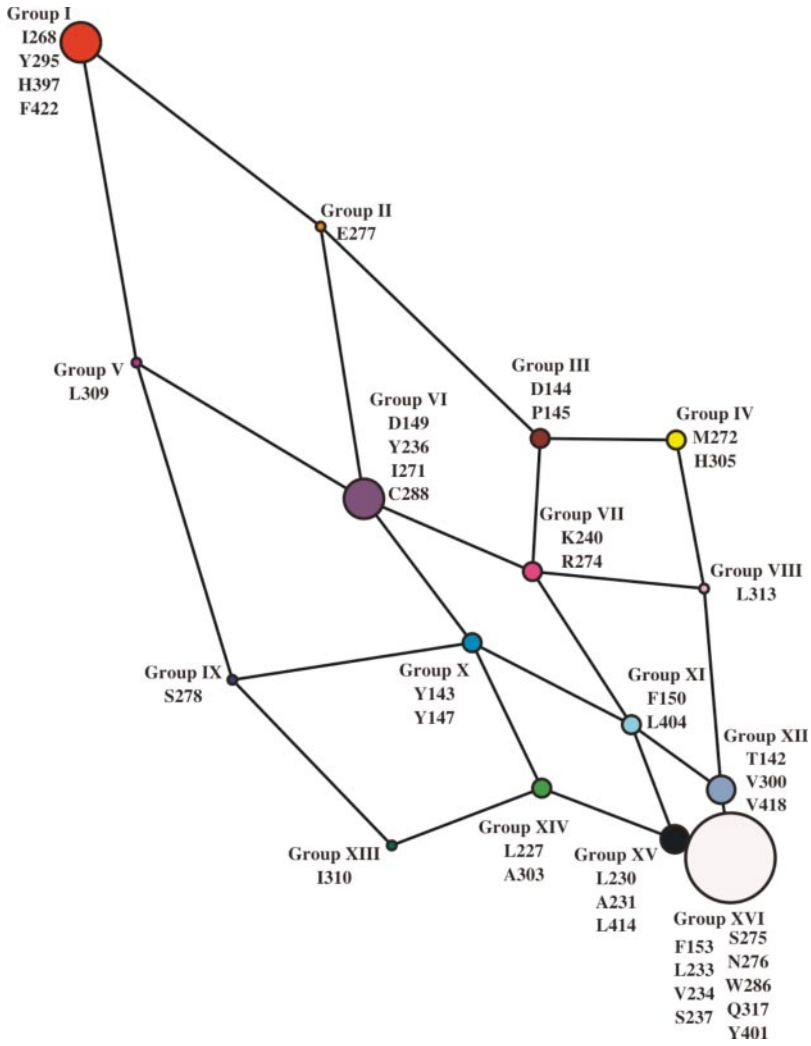

FIGURE 2. **Grouping of the amino acids forming the VDR LBP.** The 40 amino acids forming the LBP were clustered to 16 groups by using a SOM algorithm. The Sammon's mapping method allowed the visualization of the groups in two dimensions.

TABLE 1

Volume of VDR ligands and the LBPs that they create

Based on MD simulations the volumes of the four ligands (Gemini and its derivative in their two conformations) and their respective LBPs were calculated using Sybyl and Voidoo software. The absolute values in $Å^3$ as well as relative values in reference to those of $1\alpha,25(OH)_2D_3$ are indicated. From these values the percent filling of the LBP with ligand was calculated.

Ligands	Volume of the ligands	Volume of the ligands	Volume of the LBP (probe radius 1.90 Å)	Volume of the LBP (probe radius 1.90 Å)	Filling of the LBP with ligand
	Å^3	%	*Å*^{3}	%	%
$1\alpha,25(OH)_2D_3$	434.0	100.0	776.4	100.0	55.9
MC1288	427.3	98.5	643.0	82.8	66.5
Gemini I	522.5	120.4	832.3	107.2	62.8
Gemini II	519.1	119.6	919.6	118.5	56.4
Ro43–83582 I	537.2	123.8	795.8	102.5	67.5
Ro43–83582 II	541.7	124.8	850.4	109.5	63.7

Interestingly, conformation I and II of Ro43-83582 created very similar deformations of the LBP, which is comparable to the LBP of Gemini in conformation II. The consequence is a relocation of Phe-422 by 2.47 Å, His-397 by 1.76 Å, Leu-309 by 3.70 Å, and of Tyr-295 by 2.88 Å to release the pressure created by the side chain of the ligand in conformation I. The LBP expansion induced by conformation II of Ro43-83582 resulted in major movements of Leu-309 (3.83 Å) and Leu-313 (2.36 Å, data not shown). Taken together, the shrinking of the LBP in the complex with MC1288 and its expansion to accommodate the second side chain of Gemini or Ro43-83582 are the combined result of minor movements of multiple residues and major movements of a few critical amino acids.

In Vitro Analysis of Critical Residues in the VDR LBP—The point mutants F150A, Y295A, A303V, L309A, L309F, H397A, and F422A were created to test our model of the LBP in different *in vitro* assays. The mutated amino acids were the same set of representative residues as highlighted in Fig. 3. In transiently transfected MCF-7 human breast cancer cells we compared the ability of VDR_{wt} and its mutants to mediate transactivation from four copies of a DR3-type VDRE after a treatment with solvent, $1\alpha,25(OH)_2D_3$, MC1288, Gemini, and Ro43-83582 (Fig. 4*A*). The relative luciferase activity showed that with the exception of some reductions observed with Y295A and F422A none of the mutants significantly affected the basal level. In contrast, with the exception of L309F all mutants drastically lost their inducibility by

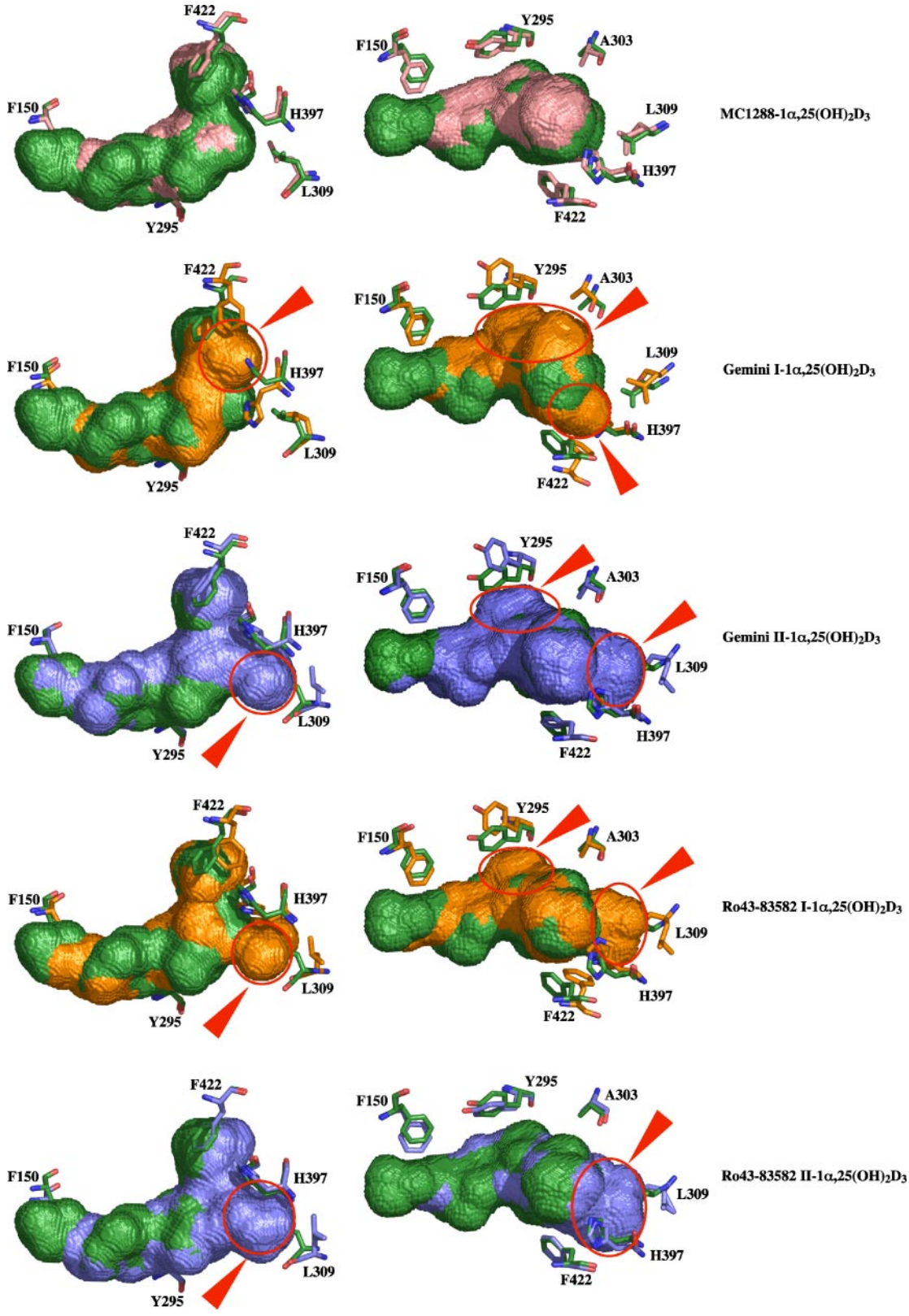

FIGURE 3. **Modulation of the LBP volume by 1α,25(OH)$_2$D$_3$ and its analogues.** Iso-surface representations of the LBPs of the complexes of VDR with 1α,25(OH)$_2$D$_3$ (*green*), MC1288 (*light brown*), and Gemini (in conformation I (*orange*) and II (*blue*)) were calculated with Voidoo software. Then the LBP of 1α,25(OH)$_2$D$_3$ was superimposed with each of the five others. *Red circles* and *arrows* mark the regions of most drastic differences between the superimposed LBPs. In addition, the movement of the representative amino acids His-397, Phe-422, Leu-309, Tyr-295, Ala-303, and Phe-150 is indicated in the same color code. The *left* and the *right panels* represent the same LBPs turned by 90°.

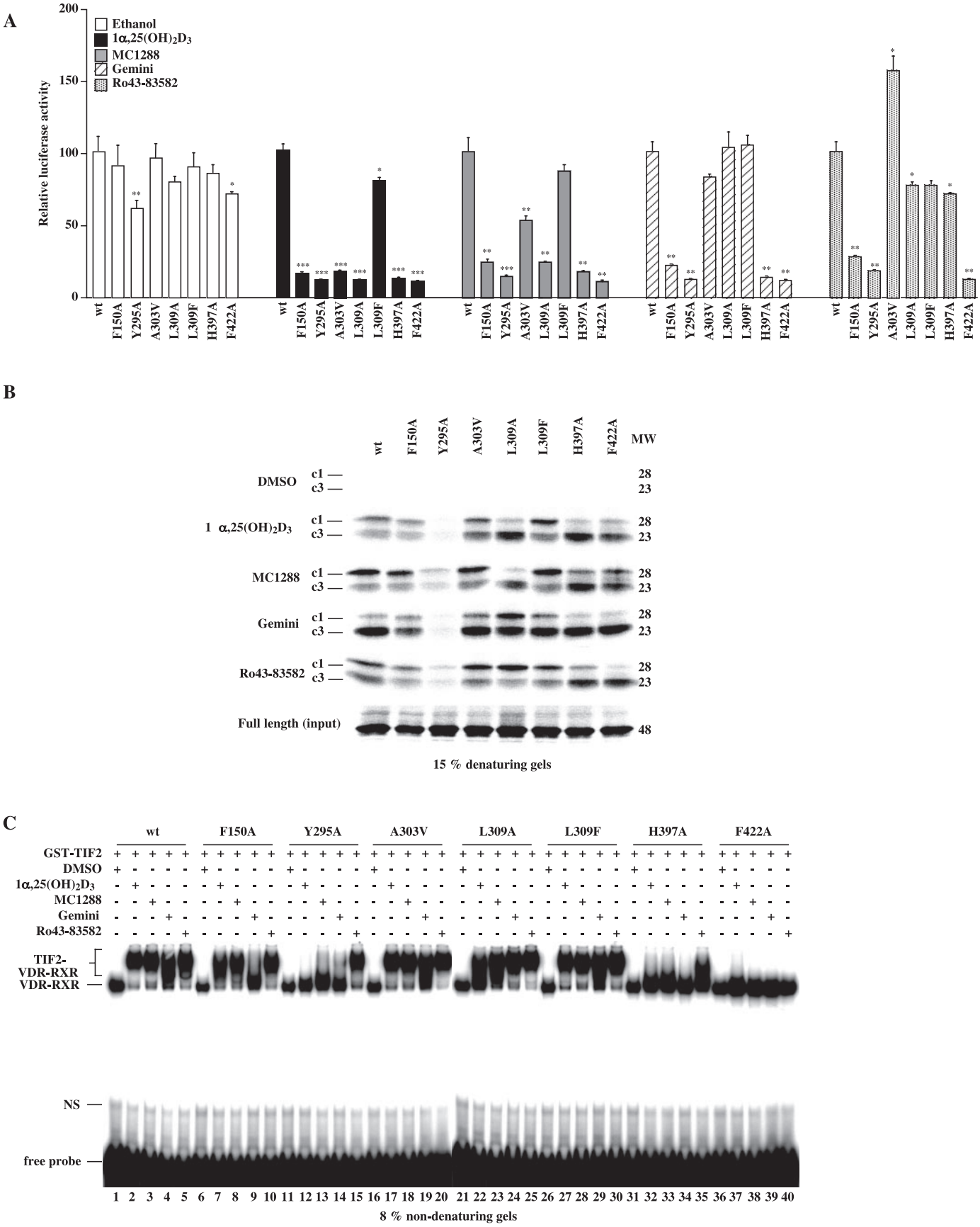

FIGURE 4. **Mutational analysis of critical residues within the LBP.** Luciferase reporter gene assays were performed with extracts from MCF-7 human breast cancer cells that were transfected by a reporter gene construct driven by four copies of the rat *ANF* DR3-type VDRE and an expression vector for VDR_{wt} or the indicated VDR mutants (*A*). Cells were treated for 16 h with solvent, 1 nM of $1\alpha,25(OH)_2D_3$, MC1288, Gemini, or Ro43-83582. For each stimulation condition the luciferase activity of the mutants was expressed in reference to the

1α,25(OH)$_2$D$_3$. With most of the VDR mutants the inducibility by MC1288 was affected but only to 50% with A303V and not at all with L309F. The induction with Gemini was clearly reduced with F150A, Y295A, H397A, and F422A, but not affected with A303V, L309A, and L309F. Finally, the response to Ro43-83582 was clearly reduced with F150A, Y295A, and F422A, slightly reduced with L309A, L309F, and H397A, and increased by 50% with A303V. In short, A303V, L309A, and H397A showed agonist-selectivity in reporter gene assays, which fits with their profile as members of the group I–III of high flexible residues surrounding the aliphatic side chain.

Limited protease digestion assays monitor the conformation in which the VDR was at the moment of a protease "snapshot." The assay is traditionally performed in a DNA-independent fashion, when the receptor is not in complex with DNA, RXR, and CoA. Most VDR ligands predominantly stabilize a large fragment of the VDR LBD (c1, from Arg-173 to the C terminus at position 427) (35) indicating the agonistic receptor conformation, whereas the smaller fragment (c3, from Arg-173 to Arg-391) (36) represents the inverse agonistic conformation. 1α,25(OH)$_2$D$_3$, MC1288, and Ro43-83582 stabilized most of the VDR$_{wt}$ molecules in c1, in keeping with their agonistic profile (Fig. 4*B*). In contrast to this observation, Gemini preferentially stabilized VDR$_{wt}$ in c3, which is characteristic for an inverse agonist. With 1α,25(OH)$_2$D$_3$ L309F showed the strongest c1 signal, with MC1288 A303V and L309F were the best, and with Ro43-83582 A303V, L309A, and L309F were most potent. However, in the presence of Gemini most mutants stayed in the inverse agonistic conformation, and only A303V, L309A, and L309F showed the tendency to stabilize the receptor also in the agonistic conformation. Interestingly, Y295A showed with all ligands an increased sensitivity to trypsin, which indicates that this mutant may lead to a general destabilization of the LBD. Taken together, the functional profile of the VDR mutants in the limited protease digestion assay resembled that of the reporter gene assays (Fig. 4*A*).

Supershift assays were performed to characterize the ligand-induced interaction between VDR and CoA protein (Fig. 4*C*). With VDR$_{wt}$ all four ligands were able to induce interaction with the CoA TIF-2. This property was unaffected by the mutants A303V, L309A, and L309F. However, with the F150A mutant receptor, Gemini failed to induce the CoA contact and with both Y295A and H397A, and only Ro43-83582 mediated VDR·CoA complex formation in the presence of these mutants. Finally, none of the ligands were able to induce the interaction of the helix 12 mutant F422A with CoA protein. In summary, Ro43-83582 was shown to be the most potent VDR agonist in this selection, because it is able to activate CoA interaction of mutants that the other ligands cannot overcome.

Agonist-selective Rearrangement of Helices 6 and 7 Residues—The most flexible residues of the LBP of the VDR were found in helices 6 and 7 and the loop between them. This observation is in agreement with the preliminary crystal structure data of the zebrafish VDR·Gemini complex (22). In the structures obtained by MD simulations the hydrophobic residues Val-300, Ala-303, His-305, Leu-309, Ile-310, Leu-313, and the closely located Leu-393 and His-397 of helix 10 were highlighted for all four ligands (Gemini and Ro43-83582 in conformations I and II) (Fig. 5). The residues Val-300, Ile-310, Leu-313, and Leu-393 showed to interact with the agonist-selective amino acids Ala-303 or Leu-309, which in turn contact the C-21 and C-26 methyl-groups of all ligands and in addition the C-31 methyl-groups of Gemini and Ro43-83582. We measured the respective distances and highlighted those that are significantly closer or more distant compared with the values determined in the VDR·1α,25(OH)$_2$D$_3$ complex. Interestingly, with MC1288 only decreased distances were observed reflecting the tighter embedding of ligand in its LBP. In contrast with Ro43-83582 primarily increased distances were found that are an indication of an increased LBP volume.

The superimposed structures in tube schematic representations showed the largest deviation for both conformations of Ro43-83582 and only minor differences for MC1288. The agonist-specific rearrangements of Ala-303 and Leu-309 are visualized in the detailed structures. Of particular interest are the choice of partner VDR residues and the relative distances of the anchoring 25-OH and 30-OH groups of the ligands. The 25-OH group of 1α,25(OH)$_2$D$_3$ was coordinated by His-305 and His-397 in distances of 2.9 and 2.8 Å, which was identical with that of MC1288. This observation is in accordance with crystal structure data (18, 19). In contrast, the 25-OH group of Gemini in conformation I interacted with Ala-303 (2.9 Å) and its 30-OH group with His-305 (3.1 Å) but not with His-397. It should be noted that in the latter structure Phe-422 is repositioned (Fig. 3), and subsequently helix 12 cannot be stabilized in the agonistic conformation. Interestingly, the interactions of the 25-OH group of Gemini in conformation II resembled very much that of the natural ligand with distances of 2.9 and 3.0 Å to His-305 and His-397; the 30-OH group contacted His-305 in a distance of 3.4 Å. The 30-OH group of Ro43-83582 in conformation I had a distance of 2.8 Å to His-305 but no contact with His-397, whereas the 25-OH group interacted with the backbone of Leu-309 (3.2 Å). Finally, the 25-OH group of Ro43-83582 in conformation II interacted with both His-305 and His-397 at distances of 2.9 and 3.0 Å, respectively. Interestingly, the 30-OH group did not directly contact any residue in the LBP, and it is probably stabilized via hydrophobic interactions or a water molecule.

Taken together, the detailed analysis of amino acids located close to the loop between helices 6 and 7 and in helix 11 revealed their individual role in contacting the 25-OH and 30-OH groups of the different agonists. This finding is consistent with the mutational analysis *in vitro* (Fig. 4) and the visualized conformation-specific stabilization of the two side chains of Gemini and Ro43-83582.

DISCUSSION

The available crystal structure data on the complexes of VDR with a collection of agonists (18–21) have been unable to explain superagonistic actions in general and agonist-selective functional profiles in particular. Reasons for the apparent unique way of agonist binding to the VDR LBD could be that the crystal structures by their nature represent minimum energetic states of the dynamic complex between ligand and receptor. In this study we aimed to overcome these problems by using the power of MD simulations and a VDR LBD complexed with a CoA peptide. To allow best comparisons between the agonist-induced effects in the VDR LBD structures and to avoid effects being related to individual modifications of the side chains, we had chosen agonists with

activity of VDR$_{wt}$. *Columns* represent the mean of triplicates, and the *bars* indicate S.D. A two-tail, paired Student's *t* test was performed, and *p* values were calculated in reference to stimulation of VDR$_{wt}$ (*, $p < 0.05$; **, $p < 0.01$; ***, $p < 0.001$). Limited protease digestion assays were performed by preincubating *in vitro* translated ^{35}S-labeled VDR$_{wt}$ or VDR mutants with solvent, 1 μM 1α,25(OH)$_2$D$_3$, MC1288, Gemini, or Ro43-83582 (*B*). After digestion with trypsin, the ligand-stabilized VDR conformations c1 (agonistic) and c3 (inverse agonistic) were electrophoresed through 15% SDS-polyacrylamide gels. Representative experiments are shown. Full-length controls confirmed equal amount of translated protein. Supershift experiments were performed with heterodimers of *in vitro* translated VDR$_{wt}$ or VDR mutants with RXRα that were preincubated in the presence of bacterially expressed GST-TIF2$_{646-926}$ with 1 μM 1α,25(OH)$_2$D$_3$, MC1288, Gemini, or Ro43-83582 and the ^{32}P-labeled rat *pit-1* DR4-type VDRE (*C*). Protein·DNA complexes were separated from free probe through 8% non-denaturing polyacrylamide gels. A representative experiment is shown. *NS* indicates nonspecific complexes. *DMSO*, Me$_2$SO.

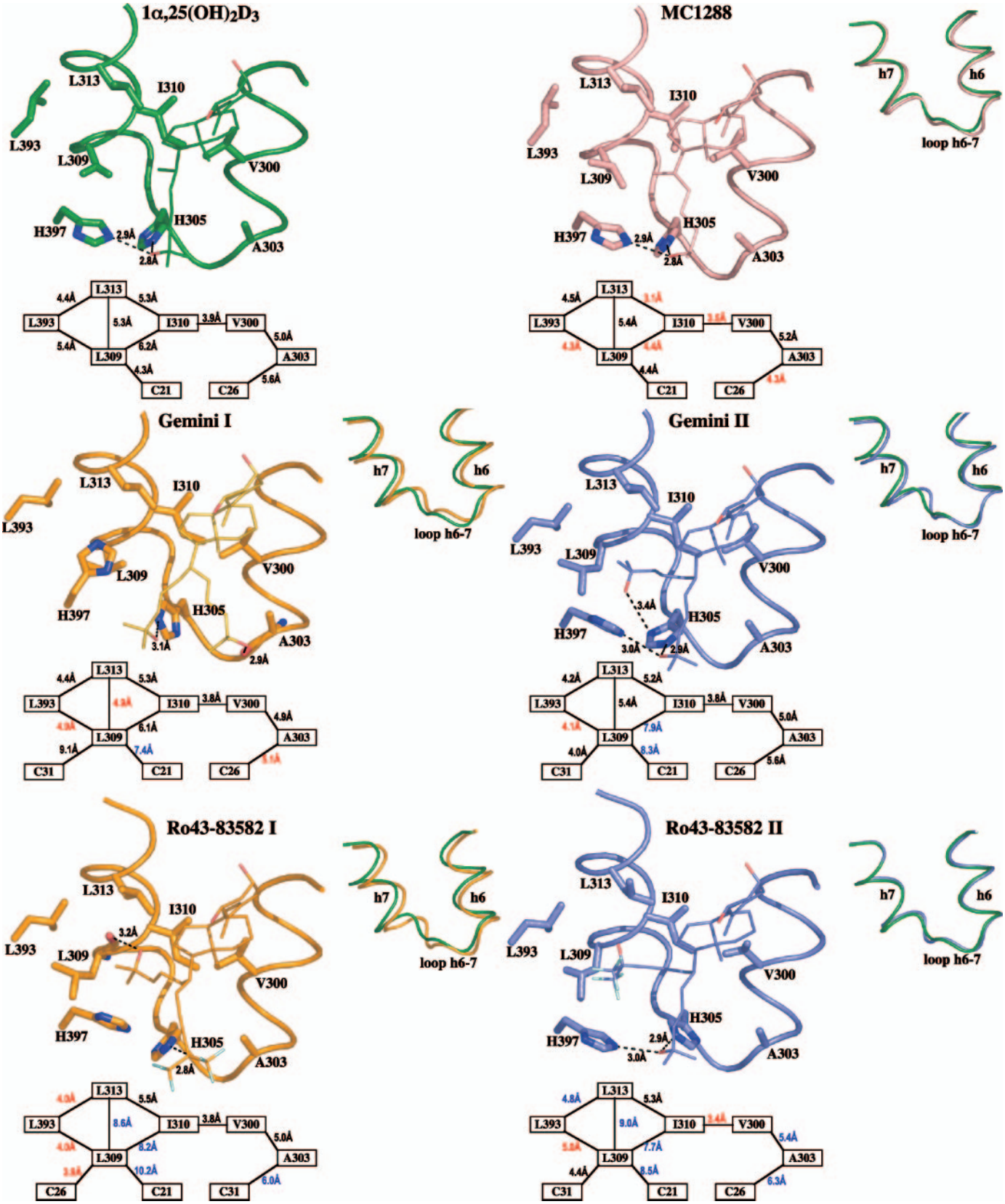

FIGURE 5. **Agonist-selective rearrangement of helices 6 and 7 residues.** Helices 6, 7, and 10 form a subregion of the VDR LBD, in which the closely located hydrophobic residues Val-300, Ala-303, His-305, Leu-309, Ile-310, Leu-313, Leu-393, and His-397 were highlighted. The ligands and their different conformations are color-coded. *Green*, 1α,25(OH)$_2$D$_3$; *light brown*, MC1288; *orange*, Gemini and Ro43-83582 in conformation I; *blue*, Gemini and Ro43-83582 in conformation II. *Dashed lines* indicate the distance of the 25-OH and 30-OH groups of the ligands to the closest residues. Please note that the structures were obtained by MD simulations based upon existing crystallographic data sets. The distances of the residues to each other and to the C-21 and C-26 of the ligand are displayed in simplified flow charts below the structures. Significantly (0.3 Å or more) decreased and increased distances (in reference to 1α,25(OH)$_2$D$_3$) are highlighted in *red* and *blue*, respectively. Tube schematic representations of the superimposed VDR LBD subregion are shown in the respective *upper right corners*.

unmodified side chains, such as 1α,25(OH)$_2$D$_3$, MC1288, and Gemini. With Ro43-83582 we use a superagonist carrying a modified side chain with high receptor binding affinity due to the six electronegative fluorine atoms at C-31 and C-32. In addition this compound contains a triple bond between C-28 and C-29 making the second side chain rather rigid.

According to our structural analysis the molecular origin of the superagonistic profile of MC1288 compared with 1α,25(OH)$_2$D$_3$ is a region between helices 6 and 7, which shows the most flexible differences between the simulated receptor·ligand complexes. This region is located opposite to helix 12, and both together serve as a roof to the LBP. The four hydrophobic residues Val-300, Ile-310, Leu-313, and Leu-393 (helix 11) interact with Ala-303 and Leu-309, which we found to be most critical for the agonist-specific profile. Most of the distances between these six residues are shorter in the VDR·MC1288 complex compared with the VDR·1α,25(OH)$_2$D$_3$ complex (Fig. 5) suggesting tighter packing in this region. Interestingly, these differences are not visible in a comparison of the respective crystal structures (18, 19), but this lack may be related to the fact that the latter were solved in the absence of a CoA peptide.

From a mechanistic point of view Gemini and Ro43-83582 are very interesting analogues, because their extra side chain increased the ligand volume in both of their conformations by ~20 and 25%, respectively. The complexes of VDR with the two side-chain analogues also showed at the region between helices 6 and 7 the most significant differences to the VDR·1α,25(OH)$_2$D$_3$ structure. This observation is in agreement with the preliminary report on the crystal structure of the zebrafish VDR·Gemini complex (22). The hydrophobic core in the loop between helices 6 and 7 has a central importance in understanding the action of superagonists. Interestingly, this region displays the largest difference between the crystal structures of VDR and the retinoic acid receptor γ (18). In VDR this region is exposed further to the surface of the LBD and contributes to the significantly increased volume of the VDR LBP.

The most surprising observation of this study was the shrinking of the LBP of MC1288, which was found to be 17.2% smaller than that of the natural hormone. Because the volume of MC1288 is only 1.5% smaller than that of 1α,25(OH)$_2$D$_3$, the LBP of MC1288 is 66.5% more efficiently filled than that of the natural hormone (55.9%). In detail, the volume of the MC1288 LBP was reduced, because most of the 40 residues forming the LBP moved toward the ligand. Interestingly, Ro43-83582 in conformation I uses an only 2.5% increased LBP volume but has a 23.8% increased ligand volume, which results in an even more efficient filling of the LBP (67.5%). These observations suggest that an efficient occupation of the LBP of a VDR ligand correlates with its superagonistic profile. However, it has to be noted that this correlation was obtained with unmodified or terminally modified side chains. Additional changes and deformations caused by ligands may create sterical clashes that cross the threshold of the volume flexibility of the LBP. In addition, it has to be noted that the calculation of LBP volumes is not standardized. Even if the same software (Voidoo) is used, different probe radii result in different absolute volumes. With 1.9 Å, we used a larger probe radius than Rochel *et al.* (18) (1.4 Å) and a smaller grid plot set (0.5 instead of 0.7 Å). Our parameters allowed the mapping of even small bulges of the LBP so that with 776 Å^3 we calculated a 79 Å^3 larger LBP volume for the natural hormone than Rochel *et al.* (18). However, on the relative value of the LBP filling we obtained an identical value with 55.9%.

Both Gemini and Ro43-83582 are able to bind the LBP in two different conformations (Fig. 1*B*). In the case of the conformation I of Gemini, neither of the two side chains takes up the agonistic position of the side chain of 1α,25(OH)$_2$D$_3$. This is reflected by the fact that in this conformation, Gemini was shown to act as an inverse agonist (24, 37, 38). In contrast, in conformation II the first side chain of the conformation II of Gemini adopts the same agonistic position of the side chain of the natural hormone, and subsequently, in this conformation Gemini is an agonist. Interestingly, the addition of electronegative fluorine atoms in Ro43-83582 prevents the inverse agonistic conformation by directing the 25-OH or 30-OH group into the agonistic position. This enables Ro43-83582 to act in both conformations as an agonist, both of which are equally potent.

In conclusion, MD simulations allow a more sensitive analysis of VDR·agonist complexes compared with the presently available parent crystal structures. In addition, our study shows that nearly all of the 40 amino acids forming the LBP contribute to the stabilization of the agonist and the flexible shape of the LBP. However, the residues Ala-303, Leu-309, and His-397 were the most selective for the tested agonists.

Acknowledgments—We thank Drs. Lise Binderup and Milan Uskokovic for providing VDR ligands and Dr. Thomas W. Dunlop for critical reading of the manuscript.

REFERENCES

1. Chawla, A., Repa, J. J., Evans, R. M., and Mangelsdorf, D. J. (2001) *Science* **294,** 1866–1870
2. Wurtz, J. M., Bourguet, W., Renaud, J. P., Vivat, V., Chambon, P., Moras, D., and Gronemeyer, H. (1996) *Nat. Struct. Biol.* **3,** 87–94
3. Väisänen, S., Ryhänen, S., Saarela, J. T., Peräkylä, M., Andersin, T., and Maenpää, P. H. (2002) *Mol. Pharmacol.* **62,** 788–794
4. Onate, S. A., Tsai, S. Y., Tsai, M. J., and O'Malley, B. W. (1995) *Science* **270,** 1354–1357
5. Carlberg, C., Quack, M., Herdick, M., Bury, Y., Polly, P., and Toell, A. (2001) *Steroids* **66,** 213–221
6. Bourguet, W., Ruff, M., Chambon, P., Gronemeyer, H., and Moras, D. (1995) *Nature* **375,** 377–382
7. Renaud, J.-P., Rochel, N., Ruff, M., Vivat, V., Chambon, P., Gronemeyer, H., and Moras, D. (1995) *Nature* **378,** 681–689
8. Leo, C., and Chen, J. D. (2000) *Gene* (*Amst.*) **245,** 1–11
9. Heery, D. M., Kalkhoven, E., Hoare, S., and Parker, M. G. (1997) *Nature* **387,** 733–736
10. Jimenez-Lara, A. M., and Aranda, A. (1999) *J. Biol. Chem.* **274,** 13503–13510
11. Vanhooke, J. L., Benning, M. M., Bauer, C. B., Pike, J. W., and DeLuca, H. F. (2004) *Biochemistry* **43,** 4101–4110
12. Suda, T., Ueno, Y., Fujii, K., and Shinki, T. (2003) *J. Cell. Biochem.* **88,** 259–266
13. Mørk Hansen, C., Binderup, L., Hamberg, K. J., and Carlberg, C. (2001) *Front. Biosci.* **6,** 820–848
14. Carlberg, C., and Mouriño, A. (2003) *Expert Opin. Ther. Patents* **13,** 761–772
15. Bouillon, R., Okamura, W. H., and Norman, A. W. (1995) *Endocr. Rev.* **16,** 200–257
16. Herdick, M., Bury, Y., Quack, M., Uskokovic, M., Polly, P., and Carlberg, C. (2000) *Mol. Pharmacol.* **57,** 1206–1217
17. Norman, A. W., Manchand, P. S., Uskokovic, M. R., Okamura, W. H., Takeuchi, J. A., Bishop, J. E., Hisatake, J.-I., Koeffler, H. P., and Peleg, S. (2000) *J. Med. Chem.* **43,** 2719–2730
18. Rochel, N., Wurtz, J. M., Mitschler, A., Klaholz, B., and Moras, D. (2000) *Mol. Cell* **5,** 173–179
19. Tocchini-Valentini, G., Rochel, N., Wurtz, J. M., Mitschler, A., and Moras, D. (2001) *Proc. Natl. Acad. Sci. U. S. A.* **98,** 5491–5496
20. Tocchini-Valentini, G., Rochel, N., Wurtz, J. M., and Moras, D. (2004) *J. Med. Chem.* **47,** 1956–1961
21. Eelen, G., Verlinden, L., Rochel, N., Claessens, F., De Clercq, P., Vandewalle, M., Tocchini-Valentini, G., Moras, D., Bouillon, R., and Verstuyf, A. (2005) *Mol. Pharmacol.* **67,** 1566–1573
22. Ciesielski, F., Rochel, N., Mitschler, A., Kouzmenko, A., and Moras, D. (2004) *J. Steroid Biochem. Mol. Biol.* **89–90,** 55–59
23. Väisänen, S., Peräkylä, M., Kärkkäinen, J. I., Uskokovic, M. R., and Carlberg, C. (2003) *Mol. Pharmacol.* **63,** 1230–1237
24. Macias Gonzalez, M., Samenfeld, P., Peräkylä, M., and Carlberg, C. (2003) *Mol. Endocrinol.* **17,** 2028–2038
25. Weyts, F. A., Dhawan, P., Zhang, X., Bishop, J. E., Uskokovic, M. R., Ji, Y., Studzinski, G. P., Norman, A. W., and Christakos, S. (2004) *Biochem. Pharmacol.* **67,** 1327–1336

26. Carlberg, C., Bendik, I., Wyss, A., Meier, E., Sturzenbecker, L. J., Grippo, J. F., and Hunziker, W. (1993) *Nature* **361,** 657–660
27. Levin, A. A., Sturzenbecker, L. J., Kazmer, S., Bosakowski, T., Huselton, C., Allenby, G., Speck, J., Kratzeisen, C., Rosenberger, M., Lovey, A., and Grippo, J. F. (1992) *Nature* **355,** 359–361
28. Voegel, J. J., Heine, M. J. S., Zechel, C., Chambon, P., and Gronemeyer, H. (1996) *EMBO J.* **15,** 3667–3675
29. Kahlen, J. P., and Carlberg, C. (1996) *Biochem. Biophys. Res. Commun.* **218,** 882–886
30. Bayly, C. I., Cieplak, P., Cornell, W. D., and Kollman, P. A. (1993) *J. Phys. Chem.* **97,** 10269–10280
31. Kohonen, T. (1995) *Self-Organizing Maps*, 2nd Edition, Springer-Verlag, Berlin
32. Rhodes, S. J., Chen, R., DiMattia, G. E., Scully, K. M., Kalla, K. A., Lin, S.-C., Yu, V. C., and Rosenfeld, M. G. (1993) *Genes Dev.* **7,** 913–932
33. Peleg, S., Sastry, M., Collins, E. D., Bishop, J. E., and Norman, A. W. (1995) *J. Biol. Chem.* **270,** 10551–10558
34. Nayeri, S., Mathiasen, I. S., Binderup, L., and Carlberg, C. (1996) *J. Cell. Biochem.* **62,** 325–333
35. Quack, M., and Carlberg, C. (1999) *Mol. Pharmacol.* **55,** 1077–1087
36. Carlberg, C. (2003) *J. Cell. Biochem.* **88,** 274–281
37. Bury, Y., Herdick, M., Uskokovic, M. R., and Carlberg, C. (2001) *J. Cell. Biochem.* **81,** 179–190
38. Herdick, M., and Carlberg, C. (2000) *J. Mol. Biol.* **304,** 793-801

S1: Distances between the OH-groups of the four VDR agonists

The distances between the 1-OH- and 25-OH-groups were determined for the MD simulation complexes of VDR with each of the four ligands. In addition, for Gemini and Ro43-83582 the distance between their 1-OH- and 30-OH-group and their 25-OH- and 30-OH-group were measured for both conformations.

Ligand	1-OH and 25-OH (1st side chain)	1-OH and 30-OH (2nd side chain)	25-OH and 30-OH (1st and 2nd side chain)
1α,25(OH)$_2$D$_3$	13.26 Å	-	-
MC1288	12.93 Å	-	-
Gemini I	13.47 Å	12.59 Å	5.91 Å
Gemini II	13.14 Å	14.49 Å	5.70 Å
Ro43-83582 I	14.12 Å	13.01 Å	8.53 Å
Ro43-83582 II	13.25 Å	13.20 Å	7.56 Å

The OH-groups of VDR ligands act as anchors within the LBP. The distance of the 1-OH-group of the A-ring and the 25-OH-group of the side chain is a sensitive parameter for differences in the VDR-ligand complexes. We therefore determined this distance in the MD simulation complexes of VDR with the four agonists. Interestingly, the shortest distance of 12.93 Å was found in MC1288. In Gemini, Ro43-83582 and 1α,25(OH)$_2$D$_3$ larger distances were measured indicating a different agonistic character of these ligands. In addition, we measured for Gemini and Ro43-83582 the distances between their 30-OH-group and either their 1-OH- or their 25-OH-group. The distances of the 1-OH- and 30-OH-group were with 12.59 and 13.01 Å for conformation I and with 14.49 and 13.20 Å for conformation II of Gemini and Ro43-83582 suggesting the equally good agonistic profile for both conformations of Ro43-83582. In contrast, both Gemini conformations indicated by the nearly identical distance of 5.91 and 5.70 Å between their 25-OH- and 30-OH-group that both groups took comparable relative positions. The two conformations of Ro43-83582 demonstrated with 8.53 and 7.56 Å rather constant distance between their 25-OH- and 30-OH-groups. This larger distance reflects a different relative position compared to Gemini.

In summary, the short distance of the anchoring 1-OH- and 25-OH-group of MC1288 suggest that this ligand is a better agonist than Gemini in conformation II and 1α,25(OH)$_2$D$_3$. In addition, the more favorable large distance between the 1-OH- and 30-OH-group of Gemini and Ro43-83582 in conformation II indicates that in this position both ligands are more efficient agonists than in conformation I.

S2: Dynamics of amino acids forming the LBP.

On the basis of the MD simulation data for each of the 40 amino acids forming the LBP the movements of the most terminal atom(s) were measured. The distances are displayed in Å and their different scales were grey-shade coded as indicated below.

	Amino acid	MC1288	Gemini I	Gemini II	Ro43-83582 I	Ro43-83582 II
I	I268	0.73	2.94	1.33	3.45	0.44
	Y295	0.69	3.14	3.00	2.88	0.89
	H397	0.86	6.13	0.97	1.76	0.54
	F422	0.78	3.44	0.89	2.47	0.23
II	E277	1.03	3.63	0.72	2.01	1.32
III	D144	0.93	2.15	0.32	1.01	0.98
	P145	1.17	2.15	0.44	1.19	1.03
IV	M272	0.46	1.55	1.04	0.72	2.09
	H305	0.92	1.76	0.31	0.67	2.03
V	L309	0.53	1.39	2.74	3.70	3.83
VI	D149	0.79	1.66	1.38	1.79	0.67
	Y236	0.68	0.83	0.81	2.31	1.81
	I271	2.00	1.98	0.38	1.75	1.78
	C288	0.76	1.86	0.71	1.92	0.85
VII	K240	0.65	1.21	0.83	1.03	1.02
	R274	0.84	1.08	0.33	1.33	1.11
VIII	L313	0.41	0.84	0.52	0.43	2.36
IX	S278	2.07	0.60	1.84	1.66	1.30
X	Y143	0.78	1.10	1.08	1.17	1.10
	Y147	1.05	1.40	0.77	1.31	1.00
XI	F150	1.09	1.08	0.60	0.78	1.16
	L404	1.04	0.91	0.16	0.34	0.83
XII	T142	0.56	0.77	0.27	0.69	0.69
	V300	0.75	0.83	0.52	0.56	0.68
	V418	0.83	0.65	0.59	0.55	0.97
XIII	I310	2.13	0.99	0.91	1.24	0.52
XIV	L227	1.81	0.82	0.56	0.58	0.40
	A303	1.19	1.23	0.73	0.81	0.81
XV	L230	0.66	0.97	0.68	0.64	0.51
	A231	1.03	0.71	0.70	0.57	0.24
	L414	1.25	0.42	0.51	0.44	0.62
XVI	F153	0.61	0.46	0.83	0.51	0.64
	L233	0.47	0.52	0.78	0.30	0.16
	V234	0.77	0.56	0.86	0.40	0.33
	S237	0.58	0.52	0.81	0.40	0.52
	S275	0.78	0.49	1.33	0.40	0.58
	N276	0.16	0.63	0.44	0.94	0.37
	W286	0.43	0.49	0.52	0.46	0.37
	Q317	0.35	0.26	0.53	0.65	0.25
	Y401	0.72	0.60	0.54	0.33	0.08

distance 0 - 0.5 Å
distance 0.5 - 1.5 Å
distance 1.5 - 2.5 Å
distance 2.5 - 3.5 Å
distance > 3.5 Å

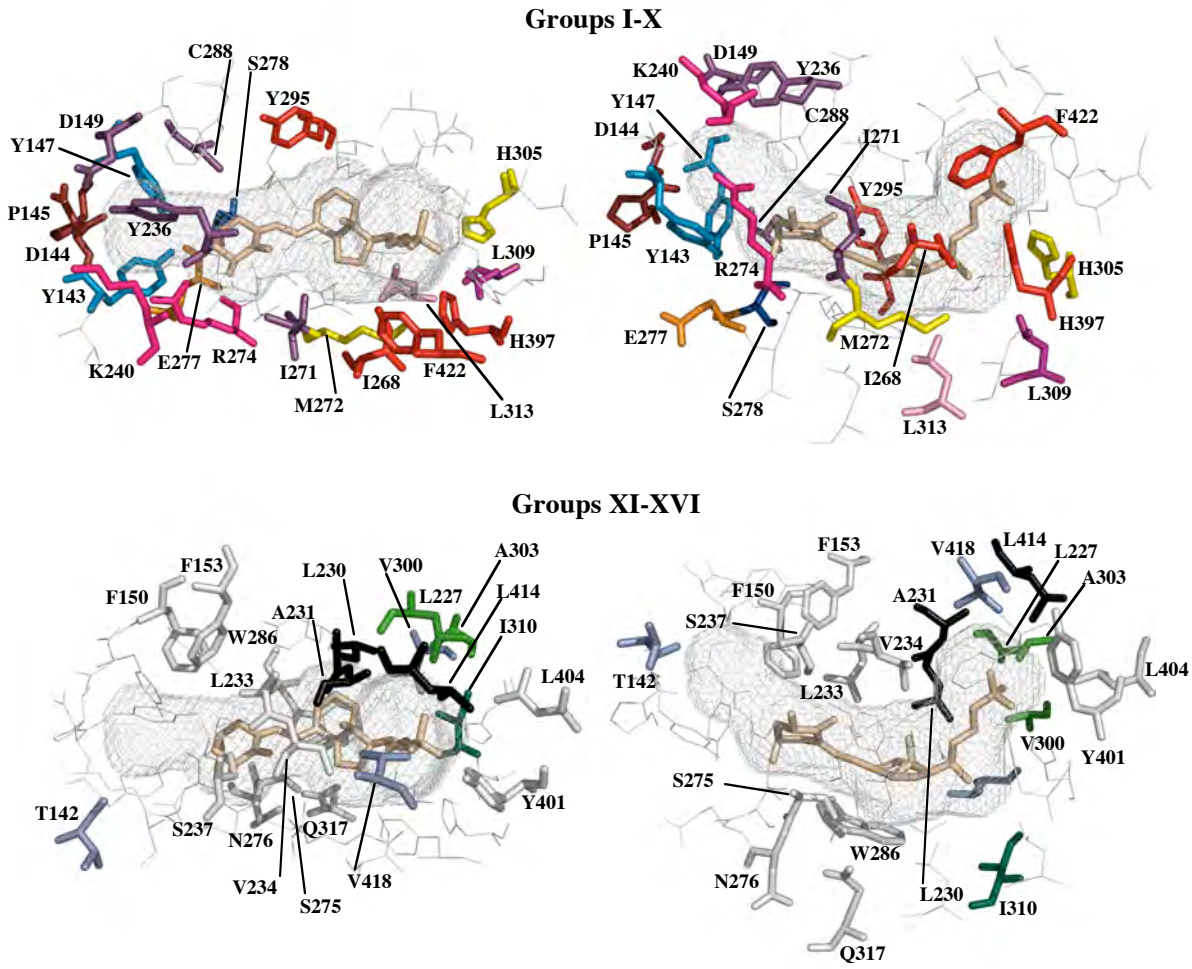

S3: Grouping the amino acid forming the LBP.

The 40 amino acids forming the LBP were clustered to 16 groups (Fig. 2). The positions of amino acids in groups I to X (top) and XI to XVI (bottom) forming the LBP of the VDR-1α,25(OH)$_2$D$_3$ structure are shown. The color code of the amino acids matches with that of the groups in Fig. 2. Interestingly, the majority of the residues of groups I to VIII are located in vicinity of the aliphatic side chains and/or the CD ring of the ligand. This observation suggests that the sub-region of the LBP around the side chain displays higher dynamics than other parts of the LBP. In contrast, the less dynamic amino acids of groups XI to XVI were found above or below the ring A- and CD-ring system. They seem to contribute to the general fixation of all of the ligands.